APPLICATION OF PASSIVE AUTOCATALYTIC RECOMBINERS FOR HYDROGEN MITIGATION: 2D NUMERICAL MODELING AND EXPERIMENTAL VALIDATION

Zanoni, M.[1], Gardner, L.[1], Gnanapragasam, N.[1] , Liang, Z.[1]
[1] Hydrogen Technologies Branch, Canadian Nuclear Laboratories, 286 Plant Rd, Chalk River, Ontario, K0J 1J0, Canada, marco.bazelattozanoni@cnl.ca, lee.gardner@cnl.ca, nirmal.gnanapragasam@cnl.ca, zhe.liang@cnl.ca

ABSTRACT

The widespread production and use of hydrogen (H_2) requires safe handling due to its wide range of flammability and low ignition energy. In confined and semi-confined areas, such as garages and tunnels, a hydrogen leak will create a potential accumulation of flammable gases. Hence, forced ventilation is required in such confined spaces to prevent hydrogen hazards. However, this practice may incur higher operating costs and could become ineffective during a power outage. Passive Autocatalytic Recombiners (PARs) are defined as safety devices for preventing hydrogen accumulation in confined spaces. PARs have been widely adopted for hydrogen mitigation in nuclear containment buildings in worst case accident scenarios, where forced ventilation is not feasible. PARs are equipped with catalyst plates that self-start due to hydrogen reacting with oxygen at relatively low concentrations (<2 vol. % H_2 in air). The heat generated from the reaction creates a self-sustained flow, continuously supplying the catalyst surface with fresh hydrogen and oxygen. In this study, a 2D transient numerical model has been developed in COMSOL Multiphysics to simulate the operation of PARs. The model was used to analyze the effect of surface reactions on the catalyst temperature, flow dynamics, self-start behaviour, forced versus natural convective flow, and steady-state hydrogen recombination rates. The model was also used to simulate carbon monoxide poisoning and its influence on the catalyst performance. Experimental data were used for model calibration and validation, showing good agreement for different conditions. Overall, the model provides novel insights into PARs operation, such as radiation and poisoning effects on the catalyst plate. As a next step, assessment of the effectiveness of PARs is underway, to mitigate hydrogen hazards in selected confined and semi-confined areas including nuclear and non-nuclear applications.

1.0 INTRODUCTION

Hydrogen (H_2) has been gaining attention as a clean fuel for transportation and energy storage with potential to eliminate the negative environmental impact of fossil fuels. However, its widespread use can pose safety concerns due to its wide range of flammability and low ignition energy. H_2 mitigation has been extensively studied in the nuclear industry [1]. H_2 can be generated during reactor core degradation, and in the case of ex-vessel molten core concrete interaction, both H_2 and carbon monoxide (CO) can be produced. The accumulation of flammable gases in the containment building can pose a threat to its integrity. Therefore, mitigation measures are critical in post-accident nuclear containments.

Canadian Nuclear Laboratories (CNL) had developed catalyst for recombining hydrogen with oxygen in oxygen streams used in the nuclear industry. The same catalyst is used for Passive Autocatalytic Recombiners (PARs) which are widely adopted for H_2 mitigation in the nuclear industry. PARs are constructed using a set of catalyst plates positioned next to each other inside a metal box with carefully designed entry and exit ducts or openings. PARs were designed to limit the H_2 concentration below the lower flammability limit (4% in air) and minimize the volume of combustible gas. The catalyst in PARs will self-start, activating the H_2 recombination reaction with oxygen (O_2) on the catalyst surface at relatively low concentrations (<2 vol. % H_2 in air) and releasing energy. The heat generated creates a self-sustained flow, continuously supplying the surface with fresh H_2 and O_2. Therefore, they do not require external power or operator action [2, 3]. The recombination rate of a PAR depends on the catalyst surface area, H_2 and O_2 concentrations, ambient pressure and temperature, and PAR box geometry [2,

3]. The recombination rate is greater at a higher H_2 concentration with sufficient O_2 present. The number of PAR boxes installed in such facilities is generally designed to ensure that the total recombination rate of PAR is greater than the maximum H_2 generation rate during an accident. If the accidental release rate of H_2 is much greater than the total recombination rate of the PARs installed, the local H_2–air mixture could become flammable. The overpressure caused by the H_2 combustion may adversely affect the facility integrity. In general, the overpressure from deflagrations at H_2 concentrations below 8% (i.e., 6-8%) without significant turbulence are tolerable, but overpressure above that H_2 concentration range are dangerous and must be avoided [3].

Besides the nuclear application, PARs can also be applied in other confined and semi-confined areas, such as underground mining, parking garages, and road tunnels as a complementary mitigation measure to active ventilation, preventing H_2 accumulation in case of a leak. In parking garages, CO is typically released from internal combustion engine vehicles. Although the concentrations should be low (not flammable), CO may create a poisoning effect on the PAR catalyst plates as it has a high tendency for adsorption at a lower temperature (< 70 ºC), inhibiting further surface reactions [2] and posing a threat to the catalyst efficiency. Experiments performed at CNL [3] has found that the exposure of a 3% H_2-air mixture along with 0.5-1.0% CO poisoned the catalyst plate at room temperature, inhibiting H_2 recombination and resulting in no catalyst activity. When the CO concentration was decreased to below 0.2%, H_2 recombination was reactivated. The threshold for poisoning depends on the CO and H_2 concentrations, ambient temperature, and catalyst formulation.

During the operation of a PAR, several thermochemical mechanisms take place, such as chemical species transport from the bulk fluid to the catalyst surface, the reaction mechanism coupled with adsorption-desorption of species at the catalyst surface, convection of the bulk fluid through the chimney of the PAR housing, heat losses through convection and radiation, and catalyst poisoning [2]. In general, experiments are limited in capturing local mechanisms. Thus, a numerical model is typically used to improve the fundamental understanding of such complex processes and then predict the PAR performance with a wide range of conditions without the need of potentially expensive and time consuming experiments.

Several numerical models have been developed to simulate the operation of PARs [2, 4-8]. These models generally use either simple [2, 4] or complex [2, 6] chemistry for simulating the catalyst reactions. Complex chemistry with several reactions requires the solution of non-linear equations leading to computationally expensive simulations as both time steps and grid sizes often need to be sufficiently refined [5]. Prabhudharwadkar et al. [9] have compared both approaches for reactions and showed that simple reactions (i.e., single step) give reasonably good results as compared to complex mechanisms. Therefore, a single-step reaction is typically applied. In such models, the effects of inlet H_2 and CO concentrations, forced versus natural convective flows, radiative heat losses, space between catalyst plates, and CO poisoning on recombination rates of PARs have been analyzed. For example, it was found that the catalyst temperature is significantly higher at higher H_2 concentrations due to a larger release of heat [4]. Moreover, radiative heat transfer plays a significant role in predicting realistic catalyst temperatures. It was observed that models neglecting thermal radiation effects over-predicted experimental catalyst temperatures [5]. When CO is considered in the gas mixture, CO recombination with no poisoning effects typically leads to increasing temperatures due to the exothermic nature of the CO recombination. However, it was found that the CO conversion efficiency was around 65% with 10% underestimation when compared to experimental data [2]. Moreover, it was found that CO poisoning was linked to low oxygen (O_2) concentrations (≤ 6%), low catalyst temperatures (although it might still happen at temperatures around 400-540 ºC), and high pressures (affecting the adsorption/desorption equilibrium towards adsorption) [7].

In the models described in the literature, a detailed analysis on surface reactions is still not well presented. Moreover, the literature lacks models that could simulate catalyst poisoning in detail. In this study, a 2D transient numerical model was developed using COMSOL Multiphysics to simulate the PAR operation. The model analyzed flow dynamics, steady-state conversion rates, and the effect of surface reactions adopting a one-step mechanism for H_2 and CO recombination reactions along with

adsorption of species on the catalyst surface temperature. Well-established steady-state experiments were used for model calibration and validation. CO poisoning on the catalyst surface was also examined.

2.0 METHODOLOGY

2.1 Model Domain and Governing Equations

Figure 1 shows the model domain (based on the REKO-3 geometry, Figure 2), divided into three sections in the vertical direction: *i*) entrance (height of 0.18 m), *ii*) catalyst section (height of 0.17 m), and *iii*) chimney (height of 0.18 m). The heights were defined according to the dimensions of the test facility and PAR used in the JÜLICH experiments [2]. Only half of the catalyst plate and channel was modeled and a symmetry boundary condition was applied. The catalyst stainless steel plate has a length of 0.143 m and thickness of 1.5 mm. The plate was assumed to be non-porous for simplicity. Moreover, no plate deformation was assumed. The width of the channel (i.e. free space between the plates) is 8.5 mm. Forced air with fixed H_2-CO inlet concentrations was employed at the entrance and H_2-O_2 and CO-O_2 surface reactions were considered on the catalyst surface. No other reactions were considered in this study. The model governing equations along with initial and boundary conditions are presented in Tables 1 and 2.

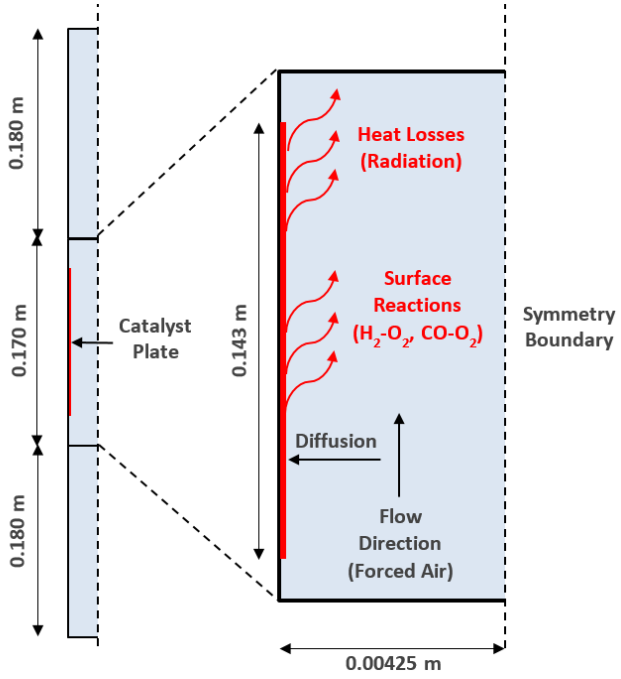

Figure 1: REKO-3 model domain.

Table 1. Model governing equations.

Single-Phase Fluid Flow	
$\nabla \cdot (\rho_i \bar{u}) = 0$, where $\bar{u}$ is the velocity vector and ρ_i is the density of each species *i*	(1)
$\rho_i \frac{\partial \bar{u}}{\partial t} + \rho_i(\bar{u} \cdot \nabla)\bar{u} = \nabla \cdot [-p\bar{\mathrm{I}} + \boldsymbol{\tau}] + \bar{F}$, where $\bar{\mathrm{I}}$ is the identity matrix, p is the pressure and $\bar{F}$ is the volume force	(2)
$\boldsymbol{\tau} = 2\mu_i \boldsymbol{S} - \frac{2}{3}\mu_i(\nabla \cdot \bar{u})\bar{\mathrm{I}}$, where μ_i is the dynamic viscosity of each species *i*	(3)
$\boldsymbol{S} = \frac{1}{2}\left(\nabla \bar{u} + (\nabla \bar{u})^{\mathrm{T}}\right)$	(4)
$\bar{F}_y = -g\rho_i$, where g is the gravity force	(5)
Heat Transfer in Fluids and Solids	

$\rho_i C_{p.i}\left(\frac{\partial T}{\partial t}+(\bar{u}\cdot\nabla)T\right)=\nabla\cdot(k_i\nabla T)$, where $C_{p.i}$ is the specific heat capacity, T is the temperature, and k_i is the thermal conductivity of each species *i*	(6)
$\rho_s C_{ps}\frac{\partial T}{\partial t}=\nabla\cdot(k_s\nabla T)$, where the subscript "s" represents "solid"	(7)
Transport of Diluted Species	
$\frac{\partial c_i}{\partial t}+\bar{u}\cdot\nabla c_i=-\nabla\cdot j_i+\dot{R}_j$, where c_i is the concentration of each species *i* and $\dot{R}_j$ is the net reaction rate of each reaction *j*	(8)
$j_i=-(D_i\nabla c_i)$, where D_i is the diffusion coefficient for each species *i*	(9)
Transport of Adsorbed and Bulk Species	
$\frac{\partial c_{s,i}}{\partial t}=-\nabla_t\cdot N_{t,i}+\dot{R}_{s,i}$, where the subscript "s" means "surface"	(10)
$N_{t,i}=-D_{s,i}\nabla_t c_{s,i}$	(11)
$\frac{\partial c_i}{\partial t}=\dot{R}_i$	(12)

Table 2. Initial and boundary conditions.

Initial Conditions	
Single-Phase Fluid Flow	
$u=0; v=V_{in}$, where V_{in} is the vertical inlet PAR velocity	(13)
$p=p_{atm}$	(14)
Heat Transfer in Fluids and Solids	
$T=T_0$	(15)
Transport of Diluted Species	
$\omega_{H_2}+\omega_{O_2}+\omega_{H_2O}+\omega_{N_2}+\omega_{CO}+\omega_{CO_2}=1$, where ω is the volume fraction	(16)
$c_{i,0}\left[\frac{mol}{m^3}\right]=\omega_{i,0}c_{tot}$	(17)
$c_{tot}=c_{H_2}+c_{O_2}+c_{H_2O}+c_{N_2}+c_{CO}+c_{CO_2}$	(18)
Transport of Adsorbed and Bulk Species	
$c_{s,i,0}\left[\frac{mol}{m^3}\right]=0$	(19)
Boundary Conditions	
Single-Phase Fluid Flow	
Wall/Catalyst plate: no slip	(20)
Inlet: $u=0; v=V_{in}$ (forced flow) $p_{in}=p_{atm}+g\rho(H)$ (buoyancy), where H is the PAR height	(21)
Outlet: $p=p_{atm}$	(22)
Heat Transfer in Fluids and Solids	
Wall: $k\nabla T=0$	(23)
Catalyst plate: $Q_b=M_{w,H_2}r_{H_2-O_2}\Delta H_{H_2O}+M_{w,CO}r_{CO-O_2}\Delta H_{CO_2}$, where r_j is the reaction rate of each reaction *j*, $M_{w,i}$ is the molar weight, and ΔH_i is the enthalpy of formation of each species *i*	(24)
Catalyst plate: $Q_{rad}=\varepsilon\sigma\left(T_{amb}^4-T^4\right)$, where ε is the effective emissivity, and σ is the Stefan-Boltzmann constant for radiation	(25)
Inlet: $T=T_0$	(26)
Outlet: $k\nabla T=0$	(27)
Transport of Diluted Species	
Wall: no flux	(28)
Inlet: $c_{i,0}\left[\frac{mol}{m^3}\right]=\omega_{i,0}c_{tot}$	(29)
Outlet: $-(D_i\nabla c_i)=0$	(30)

The model assumptions involve: *i*) the use of Navier-Stokes equations, considering incompressible flow (Equations 1 and 2), viscous stress tensor following Stokes' assumption (Equations 3 and 4), with temperature and pressure dependence on fluid properties, such as density (ρ) and dynamic viscosity (μ) estimated based on correlations described in reference [8]; *ii*) when buoyancy is assumed, a free convection flow driven by pressure difference between the inlet and outlet is initialized with no viscous stress (Equations 5 and 21); *iii*) heat transfer in fluids and solids (catalyst plate) was adopted. A heat source boundary condition via surface chemical reactions (Equation 24) and a radiative heat flux (Equation 25) were applied to the catalyst plate surface facing the bulk fluid in between the plates. Note that only a radiative heat flux was adopted for simplicity, and the convective heat flux was neglected. The effective emissivity ε was assumed as a lumped parameter that takes into account emissivity and view factor approximation; *iv*) the transport of species from the bulk fluid to the PAR catalyst plate surface considered the volume fractions of dependent variables (H_2, O_2, H_2O, N_2, CO, and CO_2). The species with the highest concentration (N_2) was used to constrain the mass for calculations to minimize the impact of any numerical errors (Equation 14); *v*) transport of adsorbed species occurs in the tangential direction along the plate surface [10, 11]. The surface molar flux, $N_{t,i}$, is governed by diffusion according to Fick's law.

2.2 Surface Reaction Kinetics

Surface reaction kinetics were based on the mass action law [10-13] for a general reaction belonging to a set of *j* reactions and involving *i* species:

$$aA + bB + \cdots \underset{k_j^r}{\overset{k_j^f}{\rightleftharpoons}} xX + yY + \cdots \tag{31}$$

For such a reaction set, the reaction rates r_j (mol/m^3·s) can be described by:

$$r_j = k_j^f \prod_{i\,\epsilon\,react} c_i^{-v_{i,j}} - k_j^r \prod_{i\,\epsilon\,prod} c_i^{v_{i,j}} \tag{32}$$

Here k_j^f and k_j^r denote the forward and reverse rate constants, respectively. The concentration of species *i* is denoted as c_i (mol/m^3). The stoichiometric coefficients are denoted by $v_{i,j}$ and are defined as being negative for reactants and positive for products. In addition to the concentration dependence, the temperature dependence of reaction rates can be included by using the predefined Arrhenius expression for the rate constants [11]:

$$k = A\left(\frac{T}{T_{ref}}\right)^n exp\left(-\frac{E}{R_g T}\right) \tag{33}$$

where A is the pre-exponential factor, E is the activation energy, R_g is the ideal gas constant, T_{ref} is the reference temperature, and T^n is the temperature factor. Thus, for H_2 and CO recombination, the reaction mechanism presented in Table 3 considered three adsorption ("ads") reactions for H_2, O_2, and CO. The $H_{2(ads)}$ and CO_{ads} then recombine (react) with adsorbed O_2.

Table 3. Initial and boundary conditions.

Reaction Mechanism	Reaction Rates (r)	Net reaction rates ($\dot{R}$)
$H_2 \underset{k_{H_2}^r}{\overset{k_{H_2}^f}{\rightleftharpoons}} H_{2(ads)}$	$r_{H_2} = k_{H_2}^f c_{H_2} - k_{H_{2(ads)}}^r c_{s,H_{2(ads)}}$	$\dot{R}_{s,H_2} = r_{H_2} - 2r_{H_2-O_2}$ $\dot{R}_{H_2} = -r_{H_2}$

$O_2 \underset{k_{O_2}^r}{\overset{k_{O_2}^f}{\rightleftharpoons}} O_{2(ads)}$	$r_{O_2} = k_{O_2}^f c_{O_2} - k_{O_2}^r c_{s,O_{2(ads)}}$	$\dot{R}_{s,O_2} = r_{O_2} - r_{H_2-O_2} - r_{CO-O_2}$ $\dot{R}_{O_2} = -r_{O_2}$
$CO \underset{k_{CO}^r}{\overset{k_{CO}^f}{\rightleftharpoons}} CO_{(ads)}$	$r_{CO} = k_{CO}^f c_{CO} - k_{CO}^r c_{s,CO_{(ads)}}$	$\dot{R}_{s,CO} = r_{CO} - 2r_{CO-O_2}$ $\dot{R}_{CO} = -r_{CO}$
$2H_{2(ads)} + O_{2(ads)} \xrightarrow{k_{H_2-O_2}} 2H_2O_{(v)}$	$r_{H_2-O_2} = k_{H_{2(ads)}}^f \left(c_{s,H_{2(ads)}}\right)^2 \left(c_{s,O_{2(ads)}}\right)$	$\dot{R}_{H_2O} = 2r_{H_2-O_2}$
$2CO_{(ads)} + O_{2(ads)} \xrightarrow{k_{CO-O_2}} 2CO_{2(g)}$	$r_{CO-O_2} = k_{CO_{(ads)}}^f \left(c_{s,CO_{(ads)}}\right)^2 \left(c_{s,O_{2(ads)}}\right)$	$\dot{R}_{CO_2O} = 2r_{CO-O_2}$

In surface reaction kinetics, the fractional surface coverages, θ_i (dimensionless) of the species (with index *i*) is described as shown in reference [11]:

$$\theta_i = \frac{\sigma_i c_{s,i}}{\Gamma_s} \tag{34}$$

where Γ_s is the density of sites of the surface as (mol/m^2) and σ_i is the site occupancy number for each species (dimensionless).

The site occupancy number accounts for the situation when a large species covers more than one site on the surface. For the case of monolayer adsorption, the sum of all fractional coverages of free and adsorbed sites is unity, and hence the fraction of free sites on the surface, θ_{free}, can be calculated from:

$$\theta_{free} = 1 - \sum_i \theta_i \tag{35}$$

2.3 PAR REKO-3 Experiments

Twenty four PAR experiments performed in the REKO-3 facilities (Figure 2) were used for model calibration and validation. The REKO-3 test facility is composed of a vertical rectangular stainless steel flow channel with a cross-sectional area of 46 mm × 146 mm. A mixture of gases containing air (O_2 and N_2), H_2, CO, CO_2, and water vapour (H_2O) passes through a catalyst section containing four catalyst plates (143 mm × 143 mm, 1.5 mm thick), where the recombination reactions (e.g., H_2-O_2 and CO-O_2) take place. The test conditions are shown in Table 4. The variable parameters include inflow velocity and inlet H_2 and CO concentrations. All the tests were conducted at an initial temperature of 25 °C and pressure of 1 atm.

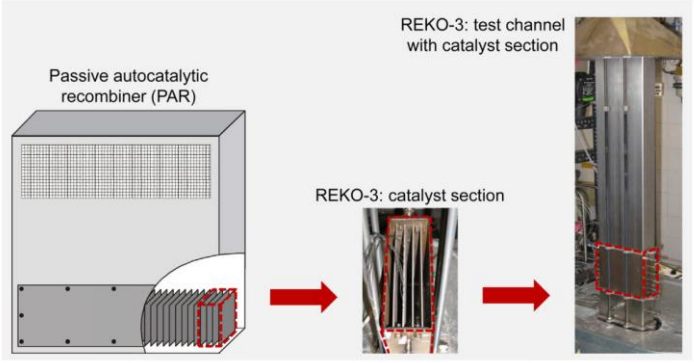

Figure 2: Schematic of REKO-3 facility [2].

The experiments followed the methodology described in Reference [2]. A mixture of air and H_2 with concentrations of H_2 varying in steps from 2.0 to 5.0% was supplied into the channel by a forced flow at 0.5 or 1 m/s. H_2-O_2 recombination takes place at the catalyst surface, releasing steam and heat and therefore increasing the catalyst and gas temperatures in that region. Steady state temperatures were typically reached after approximately 25 min. CO was then injected at concentrations varying in steps from 0.5% to 4.0%, while the H_2 concentrations were kept constant. The high catalyst temperatures caused by the H_2-O_2 reaction favour the CO-O_2 reaction, which releases more heat into catalyst plate, resulting in a temperature increase that varies stepwise according to the injected CO concentration. The catalyst temperatures are measured at different locations on both (inner and outer) plate sides. Gas concentrations were measured immediately above the catalyst plates (referred to as PAR outlet).

Table 4: REKO-3 experiments.

Experiment (#)	Forced Inlet Velocity (m/s)	$H_{2,in}$ (vol.%)	CO_{in} (vol.%)
1, 2, 3, 4	0.5	2.0	0.0, 0.5, 1.0, 2.0
5, 6, 7, 8	1.0	2.0	0.0, 0.5, 1.0, 2.0
9, 10, 11, 12	0.5	4.0	0.0, 1.0, 2.0, 4.0
13, 14, 15, 16	1.0	4.0	0.0, 1.0, 2.0, 4.0
17, 18, 19, 20	0.5	5.0	0.0, 1.0, 2.0, 3.0
21, 22, 23, 24	1.0	5.0	0.0, 1.0, 2.0, 3.0

3.0 RESULTS AND DISCUSSIONS

3.1 Model Calibration and Validation

The model calibration and validation are presented in Figure 3. The calibration was conducted by adjusting a few parameters, such as $A_{H_2-O_2}$, A_{CO-O_2}, ε, σ_{H_2}, σ_{CO}, σ_{O_2}, Γ_s, D_{s,H_2}, D_{s,O_2}, $D_{s,CO}$ to match the experimental results. Experiment # 13 ($H_{2,in}$ = 4%, CO_{in} = 0%, V_{in} = 1 m/s, Table 4) was chosen for calibrating radiation, chemical, and surface parameters of the H_2-O_2 recombination reaction, whereas experiment # 15 ($H_{2,in}$ = 4%, CO_{in} = 2%, V_{in} = 1 m/s) was chosen for calibrating the chemical and surface parameters of the CO-O_2 reaction.

Figure 3b shows that the calibrated model can reproduce the experimental catalyst temperatures well at CO_{in} = 0% (black squares vs solid black line) and CO_{in} = 2% (blue triangles vs solid blue line). Note that multiple experimental data points at a given height indicates temperature measured at the inner and outer sides of the catalyst plate. The catalyst temperature is higher at the base of the catalyst plate, increasing to a peak and then decreasing at the top. This behaviour has also been observed in the literature [5, 14]; however, details have not been provided. It is hypothesized that this initial temperature increase at the base of the catalyst plate is likely due to heat transfer edge effects between catalyst plate and air in the channel (i.e., solid and gas interface). The temperature decrease afterwards is expected as H_2 starts to recombine first at the base and then it is transported upwards at a lower concentration, which results in lower recombination rates and thus lower temperatures at the top.

After the calibration, the model was then validated (Figure 3a, c and d) against independent experiments at different air flows, $H_{2,in}$ and CO_{in} concentrations. Note that, the calibration parameters were kept constant, i.e. no further adjustments were implemented. The validation shows that the model is robust and can reproduce the independent experimental conditions well. However, the model over predicts the temperature at the base of the catalyst plate, likely because the numerical CO-O_2 recombination reaction is occurring only at the base with minor effects along the plate. The model developed in reference [2] seems to show more accurate predictions at the base of the catalyst plate.

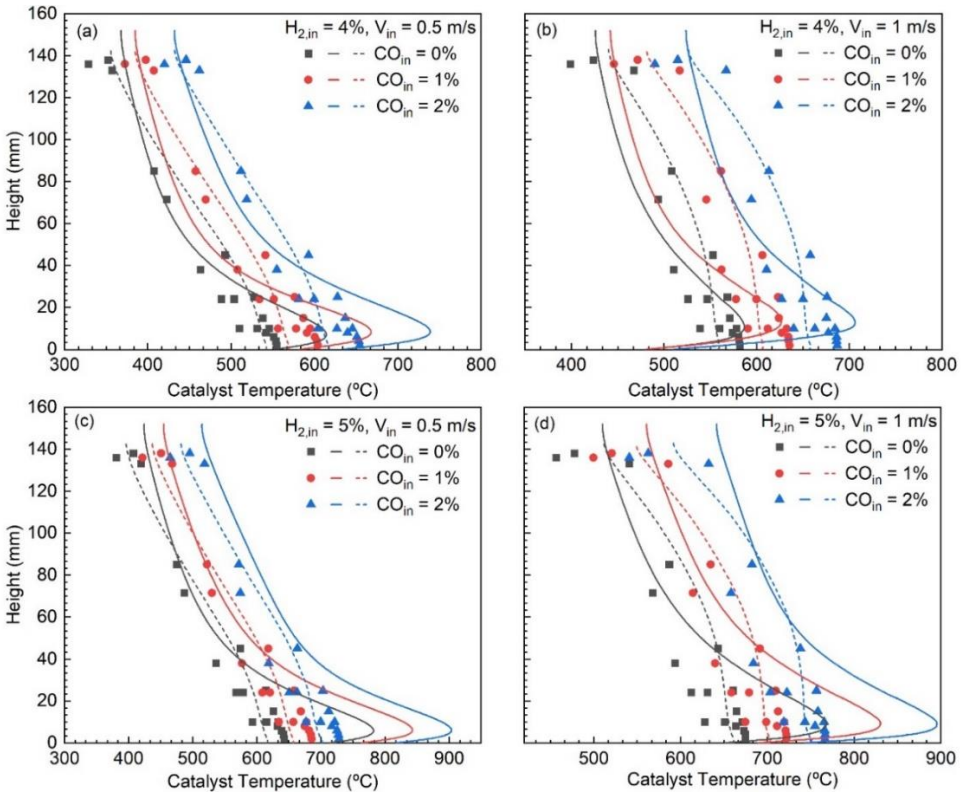

Figure 3: Experimental catalyst temperatures (symbols) covering the inner and outer sides of the catalyst plate and numerical catalyst temperatures (solid lines – this work, dashed lines –[2]) varying with catalyst height. The dashed lines are the average of the inner and outer numerical temperatures from [2].

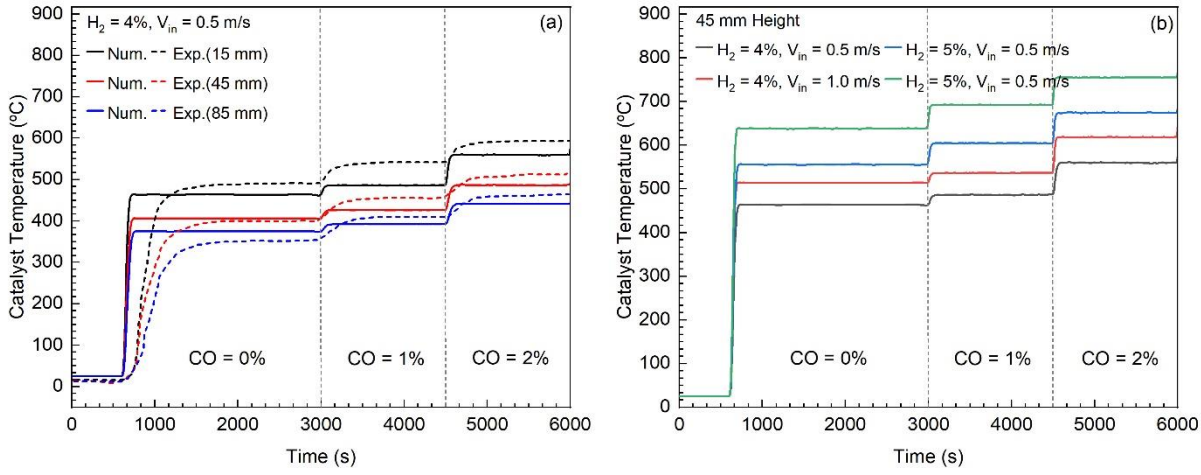

Figure 4: (a) Experimental (dashed red line) and numerical (solid line) catalyst temperature at 15, 45 and 85 mm catalyst height versus time for $H_{2,in}$ = 4 % and CO_{in} = 0-2% at V_{in} = 0.5 m/s. (b) Numerical catalyst temperature at 45 mm catalyst height versus time for $H_{2,in}$ = 4-5% and CO_{in} = 0-2% at V_{in} = 0.5-1.0 m/s.

Figure 4a shows a comparison between experimental and numerical catalyst temperature depicted at three catalyst height (15, 45, and 85 mm) for $H_{2,in}$ = 4%, V_{in} = 0.5 m/s, and CO_{in} = 0-2 %. The model is able to reproduce the steady state conditions and temperature increase due to CO injection well. Note that temperatures at this location reach steady state very quickly in the model, whereas in the experiment temperatures slowly increases until stabilization, likely due to thermal inertia of the thermocouples and

catalyst plate. This behaviour in the numerical results is likely due to boundary conditions approximations. In the model, CO injection is represented by a stepwise function, whereas in the experiment, CO concentration increases slowly, therefore, resulting in a much slower reaction rate. Moreover, note that the catalyst temperature increases with an increase in V_{in} and $H_{2,in}$ and CO_{in} concentrations (Figure 4b). This behaviour is expected as a higher air flow increases the mass flux of O_2, consequently increasing the local oxidation rates and therefore favouring more robust reactions. In addition, higher $H_{2,in}$ and CO_{in} concentrations increases the energy production, consequently increasing the temperature.

3.2 Forced versus Natural Convective Flow

Figure 5 compares the 2D contours of velocities inside the channel for forced flow (Figure 5a) and natural convection (Figure 5b, Equations 5 and 21). Thus, buoyancy is created by the pressure and density difference between the inlet and outlet. Note that the magnitude of the velocities created by the natural convection flow is very similar to the forced flow (Figure 5c), with only 6% difference. These results confirm that buoyancy was correctly simulated. The velocity increases at the catalyst height because of the high temperatures created by the recombination reactions, which changes the thermo-physical properties of air (e.g., density, viscosity, heat capacity, etc.).

3.3 Gas Temperatures, Concentrations, and Velocities in Channel (Bulk Flow Behaviour)

Figure 6a shows that the temperatures are higher at the catalyst surface, but decrease across the channel width. This behaviour is due to radiation heat transfer from the catalyst surface towards the bulk gas passing through the channel. H_2 and CO are recombined at the catalyst surface, therefore, their concentrations are lower in the channel (Figure 6b and 6c). H_2 almost completely recombines at the catalyst surface, exiting the PAR at very low concentrations (0.05%, Figure 6b). CO partially recombines, exiting the system at 1.03% (Figure 6c). O_2 concentrations decrease to 15.3% (Figure 6d), which suggests that oxygen is in excess and it is not limiting the process. CO_2 (Figure 6e) and H_2O vapour (Figure 6f) are produced during the process, increasing to 1.54% and 6.00% (14.3% close to the catalyst surface), respectively. The forced flow velocity increases from 1 m/s to 1.31 m/s due to the high temperatures at the catalyst height (Figure 6g). It then returns to 1 m/s, exiting the system. Pressures and velocities are unchanged during the process from CO_{in} = 0 to CO_{in} = 2%, which validates the approximation of incompressible flow.

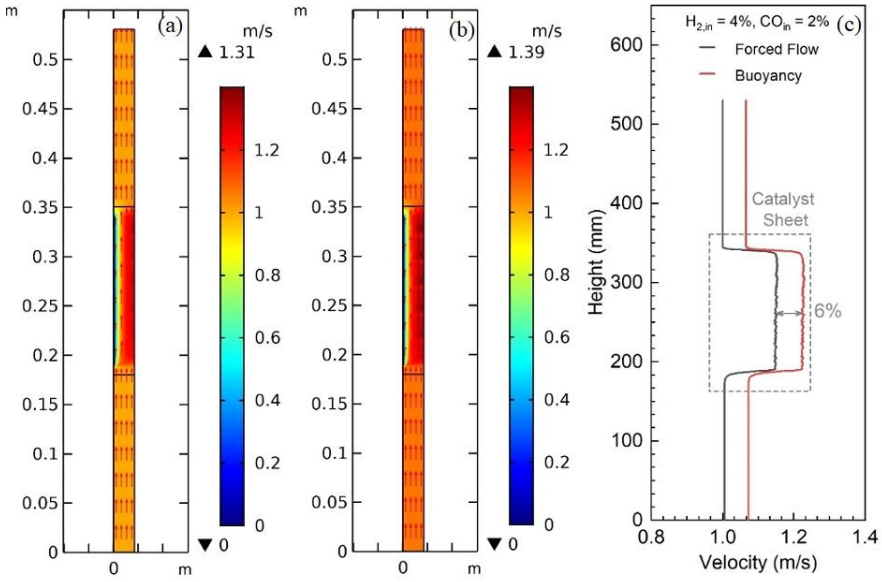

Figure 5: Velocities contours showing (a) forced air (V_{in} = 1 m/s) and (b) buoyancy conditions for H_{2in} = 4%, CO_{in} = 2%. (c) Velocity profile along the PAR height.

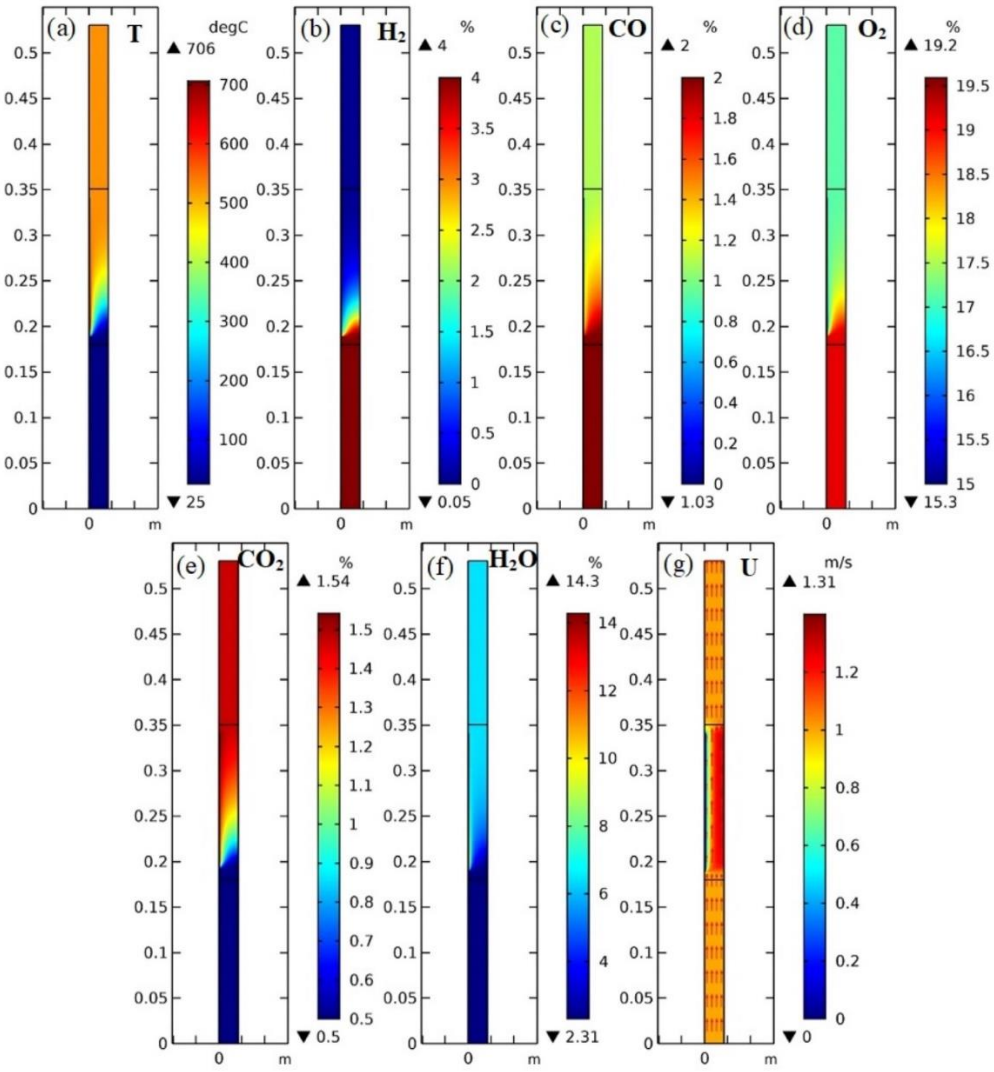

Figure 6: (a) Temperatures, (b) H_2, (c) CO, (d) O_2, (e) CO_2, (f) H_2O volumetric concentrations and (g) velocity (U) changes along PAR domain: $H_{2,in}$ = 4%, V_{in} = 1 m/s and CO_{in} = 2%. The catalyst plate is located at the heights of 0.189 and 0.341 m. The width of the channel is 4.25 mm.

3.4 CO Poisoning

CO poisoning was tested by manually increasing the parameter representing the number of sites (σ_{CO}) that CO occupies on the catalyst surface (Equation 37). This model adjustment was conducted based on a sensitivity analysis on σ_{CO} that found σ_{CO} = 6 likely resulted in CO poisoning. However, it is acknowledged that σ_{CO} = 6 might not be realistic as the CO molecule might not be large enough to occupy more than one site on the catalyst surface. When σ_{CO} = 1 (base case) and CO_{in} > 0, both H_2 and CO recombination occur.

Figure 7a shows that the catalyst temperature increases when the CO concentration increases for σ_{CO} = 1 and Figure 7b and 7e show that H_2 and CO are being consumed for this case. When σ_{CO} = 6, the catalyst temperature decreases when CO concentration increases (Figure 7d), CO recombination does not occur and H_2 recombines less (Figure 7c and 7f). This behaviour indicates that CO poisoning on the catalyst surface might be happening for σ_{CO} = 6, inhibiting H_2 recombination.

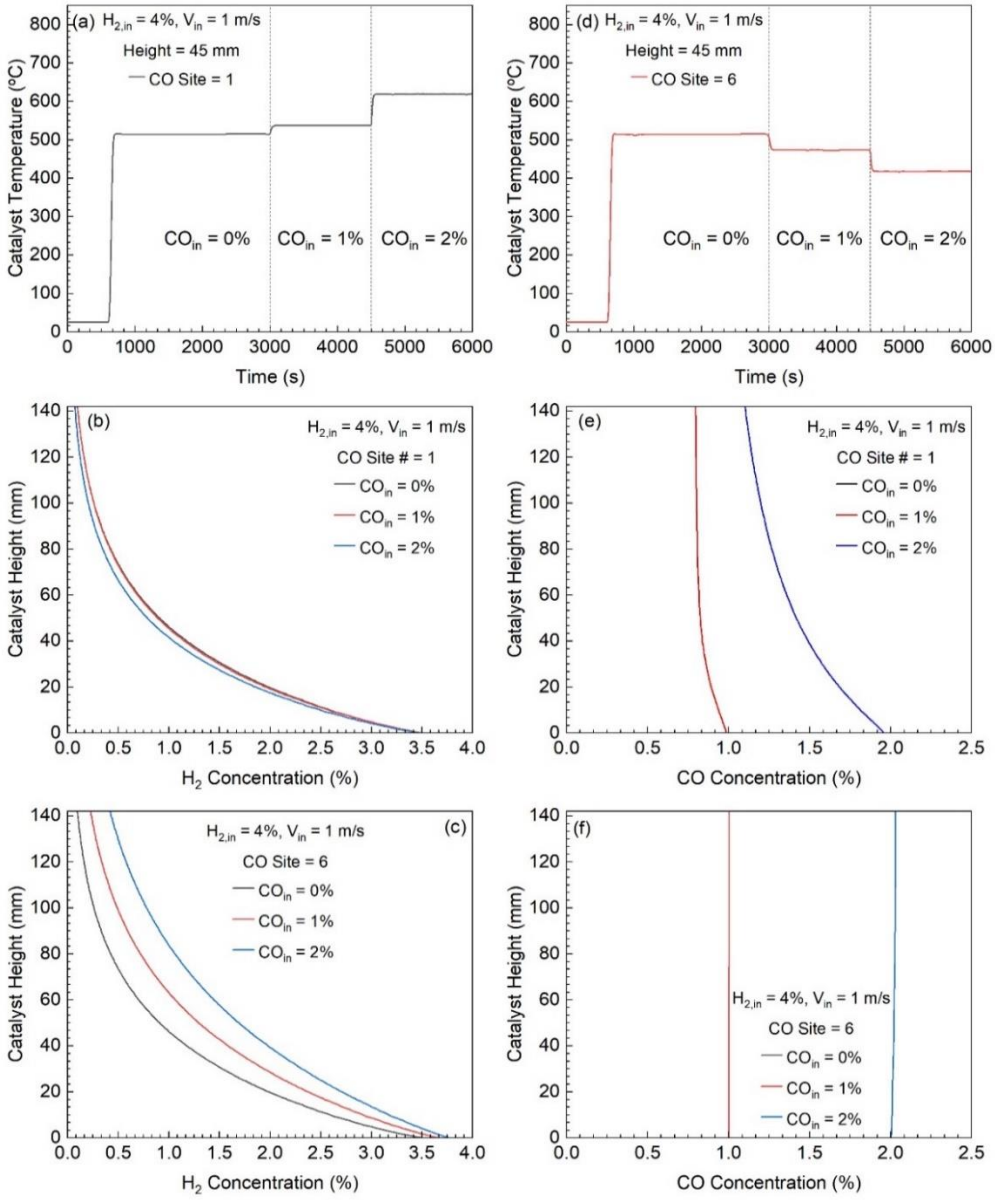

Figure 7: (a,d) Catalyst temperature at 45 mm height versus time for CO occupying 1 and 6 sites on the catalyst surface. (b, c) H_2 and (e, f) CO concentrations at the middle of the channel domain (x = 2.125 mm) varying with the catalyst height for CO occupying (b, e) 1 site and (c, f) 6 sites on the catalyst surface.

4.0 CONCLUSIONS

In this study, a 2D transient numerical model was developed using COMSOL Multiphysics to simulate the PAR operation. The model analyzed flow dynamics, steady-state conversion rates, and the effect of surface reactions adopting a one-step mechanism for H_2 and CO recombination reactions along with adsorption of species on the catalyst temperature. Well-established steady-state experiments were used for model calibration and validation. CO poisoning on the catalyst surface and forced versus natural convective flow were also examined. The model matched experimental catalyst temperature well along different conditions. However, a few model limitations were identified.

The model over predicted the temperature at the base of the catalyst plate, likely because the numerical $CO\text{-}O_2$ recombination reaction was occurring only at the base with minor effects along the plate. The model developed in reference [2] seems to show more accurate predictions at the base of the catalyst

plate. The discrepancy between the two models might be related to the chemical parameters adopted for H_2 and CO reactions, different numerical domains (with or without symmetry), and different assumptions of radiative heat losses.

Future work will focus on *i*) the fundamental understanding and accurate estimation of surface reactions and their effects on the heat release and catalyst poisoning, ii) fundamental understanding and accurate estimation of radiation heat loss and their effect on the catalyst temperature, considering the view factor approximation, *iii*) improvement of the estimation of the chemical parameters for the CO recombination, and *iv*) modification of the numerical domain to simulate the entire catalyst plate with no symmetry boundary. Overall, the model provides novel insights into PAR self-start, self-sustaining flows, H_2 and CO recombination rates, and CO poisoning. This model will be useful to assess the effectiveness of PARs to mitigate hydrogen hazards in confined and semi-confined areas.

ACKNOWLEDGEMENTS

The authors gratefully acknowledge the financial support from Atomic Energy of Canada Limited (AECL), under the auspices of the Federal Nuclear Science and Technology Program. Moreover, the authors would like to thank JÜLICH research group for providing the experimental data for model validation.

REFERENCES

1. OECD/NEA, *Status report on hydrogen management and related computer codes*. 2015, NEA/CSNI/R.
2. Klauck, M., et al., *Passive auto-catalytic recombiners operation in the presence of hydrogen and carbon monoxide: Experimental study and model development.* Nuclear Engineering and Design, 2014. 266: p. 137-147.
3. Liang, Z., L. Gardner, and T. Clouthier, *Experimental study of the effect of carbon monoxide on the performance of passive autocatalytic recombiners.* Nuclear Engineering and Design, 2020. 364: p. 110702.
4. Shukla, V., et al., *Development and validation of CFD model for catalytic recombiner against experimental results.* Chemical Engineering Journal, 2021. 407: p. 127216.
5. Raman, R.K., K.N. Iyer, and S.R. Ravva, *CFD studies of hydrogen mitigation by recombiner using correlations of reaction rates obtained from detailed mechanism.* Nuclear Engineering and Design, 2020. 360: p. 110528.
6. Meynet, N. and A. Bentaib, *Numerical Study of Hydrogen Ignition by Passive Autocatalytic Recombiners.* Nuclear Technology, 2012. 178(1): p. 17-28.
7. Klauck, M., E.A. Reinecke, and H.J. Allelein, *Effect of par deactivation by carbon monoxide in the late phase of a severe accident.* Annals of Nuclear Energy, 2021. 151: p. 107887.
8. Gnanapragasam, N., *PAR CFD Model Development to Study Catalyst Self-Start: Steady State Model Assessment and Application.* . AECL Report #153-122520-TD-002, Rev 0, 2014 March 21.
9. Prabhudharwadkar, D.M., P.A. Aghalayam, and K.N. Iyer, *Simulation of hydrogen mitigation in catalytic recombiner: Part-I: Surface chemistry modelling.* Nuclear Engineering and Design, 2011. 241(5): p. 1746-1757.
10. *Heterogeneous Chemistry*, in *Chemically Reacting Flow*. 2003. p. 445-486.
11. Coltrin, M.E., R.J. Kee, and F.M. Rupley, *Surface chemkin: A general formalism and software for analyzing heterogeneous chemical kinetics at a gas-surface interface.* International Journal of Chemical Kinetics, 1991. 23(12): p. 1111-1128.
12. *Mass-Action Kinetics*, in *Chemically Reacting Flow*. 2003. p. 371-400.
13. *Reaction Rate Theories*, in *Chemically Reacting Flow*. 2003. p. 401-443.
14. Gera, B., P.K. Sharma, and R.K. Singh, *2D numerical simulation of passive autocatalytic recombiner for hydrogen mitigation.* Heat and Mass Transfer, 2012. 48(4): p. 591-598.